

Developments in time-resolved high pressure x-ray diffraction using rapid compression and decompression

Jesse S. Smith, Stanislav V. Sinogeikin, Chuanlong Lin, Eric Rod, Ligang Bai, and Guoyin Shen

Citation: *Review of Scientific Instruments* **86**, 072208 (2015); doi: 10.1063/1.4926887

View online: <http://dx.doi.org/10.1063/1.4926887>

View Table of Contents: <http://scitation.aip.org/content/aip/journal/rsi/86/7?ver=pdfcov>

Published by the **AIP Publishing**

Articles you may be interested in

[Preface: High-pressure studies with x-rays](#)

Rev. Sci. Instrum. **86**, 071901 (2015); 10.1063/1.4926899

[New developments in laser-heated diamond anvil cell with in situ synchrotron x-ray diffraction at High Pressure Collaborative Access Team](#)

Rev. Sci. Instrum. **86**, 072201 (2015); 10.1063/1.4926895

[Development of an x-ray diffraction camera used in magnetic fields up to 10 T](#)

Rev. Sci. Instrum. **82**, 125104 (2011); 10.1063/1.3663839

[High-pressure instrument for small- and wide-angle x-ray scattering. II. Time-resolved experiments](#)

Rev. Sci. Instrum. **70**, 1540 (1999); 10.1063/1.1149621

[Rietveld analysis using a laboratory-based high pressure x-ray diffraction system and film-based detection](#)

Rev. Sci. Instrum. **68**, 2298 (1997); 10.1063/1.1148138

Frustrated by old technology?

Is your AFM dead and can't be repaired?

Sick of bad customer support?

It is time to upgrade your AFM

Minimum \$20,000 trade-in discount for purchases before August 31st

Asylum Research is today's technology leader in AFM

dropmyoldAFM@oxinst.com

OXFORD
INSTRUMENTS
The Business of Science

Developments in time-resolved high pressure x-ray diffraction using rapid compression and decompression

Jesse S. Smith, Stanislav V. Sinogeikin, Chuanlong Lin, Eric Rod, Ligang Bai, and Guoyin Shen

High Pressure Collaborative Access Team, Geophysical Laboratory, Carnegie Institution of Washington, Argonne, Illinois 60439, USA

(Received 20 February 2015; accepted 31 March 2015; published online 24 July 2015)

Complementary advances in high pressure research apparatus and techniques make it possible to carry out time-resolved high pressure research using what would customarily be considered static high pressure apparatus. This work specifically explores time-resolved high pressure x-ray diffraction with rapid compression and/or decompression of a sample in a diamond anvil cell. Key aspects of the synchrotron beamline and ancillary equipment are presented, including source considerations, rapid (de)compression apparatus, high frequency imaging detectors, and software suitable for processing large volumes of data. A number of examples are presented, including fast equation of state measurements, compression rate dependent synthesis of metastable states in silicon and germanium, and ultrahigh compression rates using a piezoelectric driven diamond anvil cell. © 2015 AIP Publishing LLC. [<http://dx.doi.org/10.1063/1.4926887>]

I. INTRODUCTION

From a conceptual viewpoint, time is arbitrary in the context of static high pressure research. Measurements are typically carried out on systems assumed to be in thermodynamic equilibrium following some effort to generate and maintain high pressure. From a practical viewpoint, time is also somewhat arbitrary during the course of a static high pressure experiment. Considering, for example, synchrotron x-ray diffraction measurements, the time required to carry out various experimental processes—x-ray exposure, detector readout, changing and measuring sample pressure, etc.—varies greatly depending on the nature of the sample, needs of the experiment, and specifications of the overall apparatus. Experimental descriptions in the literature frequently include the time required to carry out some of these various processes, but rarely are these times understood to have a direct impact on the underlying science. In short, time is not typically a relevant experimental variable in static high pressure research.

Time is an important parameter, however, for understanding many physical processes. Material properties and phase transition pathways, for example, are strongly influenced by the time dependence of various driving mechanisms (thermal transfer, strain, irradiation, etc.). By leveraging state-of-the-art capabilities for selected aspects of a high pressure experimental configuration, it is possible to carry out high pressure measurements on relatively short time scales and/or at relatively high frequencies compared to what was possible just a few years ago. Thus, it is now possible to carry out dynamic high pressure measurements using what would traditionally be considered static high pressure apparatus. Here, *dynamic* is used in a general sense meaning the time dependence of one or more experimental parameters has a significant impact on the experiment. Recognizing the emerging possibilities in time-resolved high pressure research, there has been a sustained effort at HPCAT (High Pressure Collaborative Access Team)

to develop apparatus and techniques for collecting high quality time-resolved high pressure x-ray scattering data.

In this work, we present recent developments in time-resolved high pressure x-ray diffraction combined with rapid compression and/or decompression of a sample in a diamond anvil cell (DAC). X-ray diffraction is among the most fundamental experimental methods inasmuch as the structure of materials serves as the foundation for understanding and describing material properties. The importance of x-ray diffraction is particularly salient in high pressure studies, where the application of pressure modifies a material's atomic arrangement through either a continuous change in density or an abrupt change in phase or crystal structure. Adding a time-dependent pressure component to these studies opens up the possibility of using a DAC to explore the effects of rapid (de)compression on the structure of materials including, for example, phase transition kinetics, synthesis of metastable phases, material deformation and relaxation, etc.

The effect of rapid (de)compression in the DAC has already been demonstrated in a few instances. For example, Zhao *et al.* obtained metastable phases of Si using rapid decompression¹ and Dera *et al.* suppressed the $\alpha \rightarrow \text{II}$ transition in cristobalite using rapid compression.² In each of these works, the authors estimate the (de)compression from manually turning the DAC pressure screws was achieved in ~ 100 ms (or less). A DAC with integrated piezoelectric actuators for changing sample pressure was developed specifically for compression rate dependent studies³ and has been used for micrographic and spectroscopic studies of pathway dependent phases in ice⁴⁻⁶ and crystal growth rates in hydrogen and deuterium.⁷ The developments described herein significantly expand the research possibilities in this field. For example, by adding high frequency x-ray imaging, it is possible to observe the structural progression *during* (de)compression and later quantify the (de)compression rate. By enabling larger, faster, and more controlled pressure steps, it may ultimately be

possible to obtain DAC strain rates up to and including the lowest achievable strain rates generated using shock compression apparatus.

This work is divided into two main sections: the first section addresses selected components in the overall apparatus which enable time-resolved x-ray diffraction capabilities at HPCAT. Considering all of these components together gives an indication of the accessible time scales and strain rates, and thus the kinds of scientific questions which can be addressed using these new capabilities. The second section consists of early examples and experiments demonstrating some of these new capabilities.

II. APPARATUS

Rather than giving a complete description of the beamline where a majority of this work was carried out (16-ID-B at the Advanced Photon Source (APS)), we here discuss the few specific components most relevant to the development of time-resolved x-ray diffraction with rapid (de)compression: beam delivery, sample pressure control, detectors, and data analysis software. Considering these elements together as a single apparatus helps in determining the relevant time scales and accessible strain rates at HPCAT.

A. Beam delivery

Photon flux on the sample plays a crucial role in determining the minimum exposure time required to collect an x-ray diffraction image with an acceptable signal-to-background ratio. Unfortunately, the design and operating principles of the DAC impose a number of practical limitations in terms of minimizing x-ray exposure time. Some of these limitations include microscopic scattering volumes, x-ray absorption by relatively thick diamond anvil windows, potential for unwanted scattering from gasket material surrounding the sample, and a limited optical aperture defined by the diamond anvil supports. Thus, high pressure experiments generally require the highest possible flux of high energy photons delivered to the sample via a tightly focused beam.

HPCAT's 16-ID-B is one of just a few dedicated high pressure x-ray diffraction endstations in the world which benefits from both an undulator source and a third-generation high-energy storage ring. A specific x-ray wavelength is selected by passing the quasi-monochromatic undulator beam through a cryogenically cooled silicon double-crystal monochromator. Although there are three monochromator crystal pairs available at beamline 16-ID-B, for flux-limited time-resolved experiments, we typically use the Si (111) pair to take advantage of the relatively large energy bandwidth. The beam is focused down to a few μm , typically $5 \mu\text{m}$ (vertical) \times $7 \mu\text{m}$ (horizontal) at FWHM, using a pair of 320 mm \times 320 mm Kirkpatrick-Baez mirrors,⁸ with the "tails" of the focused beam cleaned up using a pinhole aperture selectable from 15 μm to 50 μm in diameter.

Table I summarizes key beam delivery components. Much of the data presented herein were collected using an incident x-ray energy of 20.000 keV. This represents the best compromise considering flux from the source, throughput of the

TABLE I. Beam delivery components at beamline 16-ID-B.

Storage ring	Energy	7.0 GeV
	Current	100 mA
	Emittance	3.129 nm rad
Source	Type	APS undulator A
	Period	3.3 cm
	Length	2.4 m
	Peak B field	0.9 T
	Peak K value	2.8
Monochromator	Configuration	Double-crystal (+,-)
	Material	Si
	Pairs	(111), (220), (311)
	Energy range	12-42 keV
Focusing optics	Configuration	KB mirrors
	Length	320 mm
	Coatings	Rh or Pt
Clean-up	Type	Pinhole
	Sizes	15-50 μm

x-ray optics, scattering and absorption of the sample and DAC, and energy-dependent detector efficiency. On-sample flux for these experiments is on the order of 10^{11} or 10^{12} photon/s, depending on choice of energy and monochromator crystal indices.

B. Sample pressure control

For many contemporary DAC experiments, the pressure is increased just as it was for the first DAC experiments—by manually turning screws. For time-resolved experiments, it is necessary to have some sort of remote, programmable pressure control. An ideal pressure control apparatus would allow for remote, reliable, repeatable, and programmable pressure control over a wide range of pressures and time scales. Unfortunately, there is no ideal pressure control available. Several remote pressure control apparatus with relative strengths and weaknesses have been developed for various DAC designs. For the current work, we used two different pressure control apparatus: a pneumatic diaphragm and a piezoelectric actuator.

DAC pressure control using a pneumatic diaphragm was first described over 30 yr ago⁹ and has since enjoyed widespread use in the static high pressure community. Diaphragms are very similar in design and operation to membranes, and the two terms are frequently used interchangeably when referring to a pneumatic pressure control apparatus. The basic concept and some design examples have been described elsewhere.^{9,10} Until recently, diaphragm pressure control was similar to manually turning DAC screws, only instead one manually turned needle valves to increase or decrease the gas pressure in the diaphragm. Over the past few years, there has been a shift in the static high pressure community from manual gas pressure controllers toward automatic, programmable pressure controllers. This makes it possible to preset a number of parameters including the final diaphragm pressure and the rate of pressure increase. At HPCAT, we use our own diaphragm

design described elsewhere in this volume¹¹ together with PACE modular pressure controllers manufactured by GE.

A DAC with integrated piezoelectric actuator(s) for pressure modulation—the dynamic diamond anvil cell or dDAC—was first introduced⁵ and described³ just a few years ago and has since seen very limited use. Some of the key operating principles, including cyclic, repeatable pressure modulation and/or very fast (step) pressure changes, are highly desirable from a conceptual point of view but challenging to achieve in practice. Ultrafast pressure changes could provide an opportunity to study, for example, phase transition dynamics or controlled grain growth, but it may not be possible to collect sufficient scattering intensity over such short time scales. This could be overcome by repeated measurements—a sort of pump-probe approach—for which the dDAC seems well-suited. But pressure increase in a DAC comes primarily from plastic deformation of the gasket material, making the possible range of repeatable, cyclic pressure very small. Notwithstanding these challenges, we have been able to utilize our own dDAC design for cyclic, repeatable measurements over a range of a few GPa, and we have also used it to generate very high strain rates. The actuator stroke is controlled using an arbitrary-wave function generator operated from 0 to 10 V, which in turn is scaled from 0 to 1000 V using a dedicated power supply. The design and operation of the HPCAT dDAC are described in more detail elsewhere in this volume.¹¹

Increasing DAC pressure in a controlled and reliable way is fairly straightforward. A force is applied to the two opposing anvils to plastically deform the gasket and reduce the sample chamber volume with a corresponding increase in sample pressure. But because the gasket deformation is mostly plastic, it is difficult to decrease sample pressure in a similar controlled way as there is no active force driving the anvils apart. Typically as the compression apparatus (manual, pneumatic, or piezoelectric) is released, the DAC tends to stick and slip, resulting in imperceptibly small and overly large pressure steps. This method of passive sample decompression does not provide the control and reliability required for time-resolved decompression studies. To overcome this problem, HPCAT has designed decompression diaphragm and dDAC assemblies that actively drive the anvils apart, working against the opposing compression assembly. This facilitates reliable, controlled unloading of sample pressure without the sticking and slipping that is characteristic of passive unloading. The dDAC and diaphragm can each be used in either a compression or decompression configuration and can be used in combination (e.g., compression diaphragm together with decompression piezoelectric actuator) for maximum control and flexibility. Figure 1 shows a mounted DAC with dDAC assembly (right) in decompression configuration together with a membrane assembly (indicated by the small capillary pressure line left of the DAC) in compression configuration.

C. Detectors

The most recent technical advancement that has ultimately enabled time-resolved high-pressure x-ray diffraction is the development of high-frequency area detectors. The introduction of large hybrid pixel array detectors with very

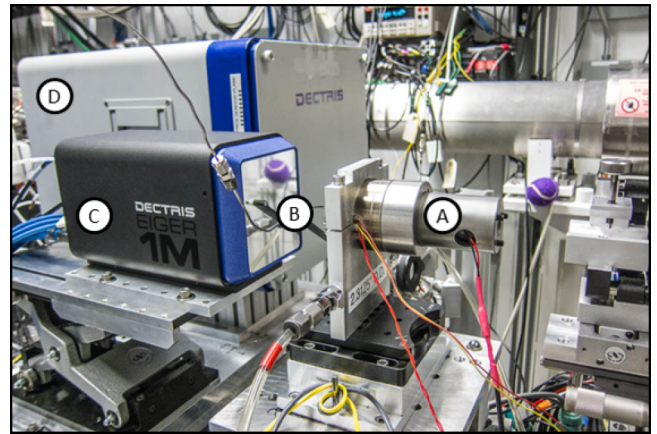


FIG. 1. Time resolved equipment. A DAC is mounted with a piezoelectric actuator (A) configured for decompression and a pneumatic diaphragm (B, indicated by the metal capillary tube) configured for compression. The DECTRIS EIGER 1M prototype (C) and PILATUS 1M (D) detectors used for the examples can be seen in the foreground and background, respectively.

short readout times on the order of milliseconds means that now instead of talking about the number of seconds, one needs to collect an image; it is now possible to talk about the number of images one can collect per second. The majority of data presented in this work were collected using a PILATUS 1M detector. Some specifications which are particularly important in the context of high pressure x-ray diffraction are presented in Table II. The maximum imaging frequency of the detector is 125 Hz. This gives a minimum acquire period (x-ray exposure time + 2.3 ms readout time) of 8 ms. For one example below (step compression for maximum strain rate), we used a prototype detector provided by DECTRIS, similar to what is now commercially available as the EIGER 1M.¹² For our tests, we operated the detector at 800 Hz. The readout time was extremely short ($\sim 20 \mu\text{s}$ for the prototype) so from a practical standpoint, the detector was continuously collecting images with $\sim 1.25 \text{ ms}$ exposure. Figure 1 shows both of these detectors as mounted in the experimental hutch.

D. Software

The nature of high-pressure x-ray diffraction is such that data often need to be qualitatively, if not quantitatively, evaluated during the course of the experiment. Phase transitions, unwanted scattering from diamond or gasket, and other image features which can drastically change during the course of an experiment mean subsequent data reduction must often

TABLE II. Selected PILATUS 1M specifications.

Sensor	Reverse-biased Si diode array
Sensor thickness	450 μm
Pixel size	172 \times 172 μm^2
Area	169 \times 179 mm^2
Dynamic range	20 bits
Readout time	2.3 ms
Framing rate	125 Hz
Point-spread function	1 pixel

be carried out on an image-by-image basis. Thus, there has been little need for automated software routines capable of processing large high pressure data sets. The high-frequency imaging capability of modern detectors, however, means that one can collect an overwhelming amount of imaging data in a matter of seconds and it is now imperative that the high pressure community has access to software tools that can facilitate and streamline rapid data reduction.

For the examples in this work, we have primarily used three software tools: Albula for on-line image viewing, Fit2d for image integration, and GSE_shell for diffraction pattern analysis. Albula is DECTRIS' free software for viewing image files collected using their PILATUS and EIGER detectors. It has straightforward (and relatively few) controls which make it easy to navigate series of diffraction images by manually "stepping" through images (choosing among convenient step sizes) or automatically displaying an image series like a movie. In short, it is a simple and convenient way to quickly and efficiently assess image quality during the course of an experiment. Fit2d was used to convert x-ray images into conventional x-ray diffraction patterns.¹³ For large series, it is not feasible to integrate each image manually, so the macro-capability was employed. For image file sizes and integration parameters used in this work, the macro could output about two x-ray diffraction pattern files per second. GSE_shell, written and developed by Dera at GSECARS (Sector 13) at the APS, was used to analyze diffraction patterns by the way of individual peak fitting to determine lattice parameter. Again, because of the large volume of data, it is not feasible to fit each pattern manually. The code was modified by its author, Dera, to automatically fit selected peaks in a series of n patterns, where the fitting results from the $(n\text{-th} - 1)$ pattern are the initial fitting parameters of the $n\text{-th}$ pattern. The results of the fit are output in text files containing a number of parameters including integrated intensity, peak position, FWHM, and peak shape (Gaussian-Lorentzian mixing parameter) for each peak, as well as unit cell and pressure (calculated from an equation of state provided by the user) for each phase.

III. EXAMPLES

The various beamline components, ancillary equipment, and software tools described in Section II together constitute a unique apparatus for carrying out time-resolved high pressure x-ray diffraction combined with rapid (de)compression. In this section, we offer several examples of experiments carried out using this apparatus. In the interest of highlighting a wide range of time scales, (de)compression rates, pressure control assemblies and configurations, strain rates, and possible types of measurement, we present some examples with limited experimental details, data sets, and/or scientific conclusions. Nevertheless, the material presented below gives a good indication of the technical capabilities and research possibilities at HPCAT.

A. Ramp compression (pneumatic)

For a first attempt at high pressure x-ray diffraction using rapid compression, we tried a "fast" equation of state

measurement at ambient temperature. The primary goal was to gain insight into various technical aspects associated with rapid compression, including the response and performance of the membrane and gas pressure controller assembly, the mechanical/positional stability of the sample assembly during rapid compression, a possible unexpected response by the diamond anvils (either early failure or increased pressure range, depending on the nature of diamond failure), the material response of the sample(s), and the feasibility of automated processing of large volumes of high pressure diffraction data.

Molybdenum and magnesium oxide were selected as sample and pressure marker because both have been studied extensively up to ultrahigh pressures and neither undergoes a structural phase transition up to at least several hundred GPa. A mix of Mo and MgO powders was loaded without pressure transmitting medium into a symmetric DAC with beveled anvils (250 μm diameter with 100 μm flats) and a rhenium gasket. Powder x-ray diffraction images were collected using a PILATUS 1M detector approximately 200 mm from the sample, using an incident x-ray energy of 20.000 keV ($\lambda = 0.61992 \text{ \AA}$). Initially, diaphragm pressure was increased and images were collected in a stepwise (conventional) manner to engage the diaphragm and then ensure the sample chamber was stable (no significant change in sample chamber size or position) upon increasing pressure. The ramp compression was carried out from an initial sample pressure of about 80 GPa. The gas pressure controller was set to increase diaphragm pressure at a rate of 35 bars/s from an initial pressure of 17 bars to a maximum pressure of 135 bars (well beyond the expected pressure for diamond failure with this particular DAC configuration). Imaging frequency was 100 Hz (7 ms exposure time during each 10 ms acquire period) set to run for a total of 1000 images (10 s). Given the limitations of the pneumatic system, it is not possible to precisely synchronize the initial increase in sample pressure with the initial x-ray image, so we manually started the imaging sequence about 1 s prior to starting the ramp compression. Catastrophic diamond failure, indicated by a loud crack from inside the experimental hutch, occurred almost immediately following the start of the pressure ramp.

Data were processed using the software and methods briefly described in Section II D. Pressure was calculated based on the equation of state of MgO.¹⁴ Figure 2 shows the results of the ramp compression. Fig. 2 (top) shows an example of an x-ray diffraction pattern obtained at ultrahigh pressure, 208 GPa. With a 7 ms exposure time, the intensity is fairly weak at just a few counts per pixel, but capturing the complete ring on the area detector still yields an acceptable signal-to-background ratio for robust peak fitting. Fig. 2 (middle) shows the sample pressure evolution over time together with the corresponding rate of increase in sample pressure. The overall pressure increase of 127 GPa was completed in 1.13 s (113 data points), giving an average compression rate of over 100 GPa/s. However, the instantaneous compression rate varied substantially throughout the ramp, from as low as 40 GPa/s near the end to as high as over 240 GPa/s at the peak rate of increase. (Note that the rate of increase was determined by differentiating a smooth polynomial fit of the $P(t)$ data.) The resulting equation of state is shown in Fig. 2 (bottom), compared with equations of state obtained under

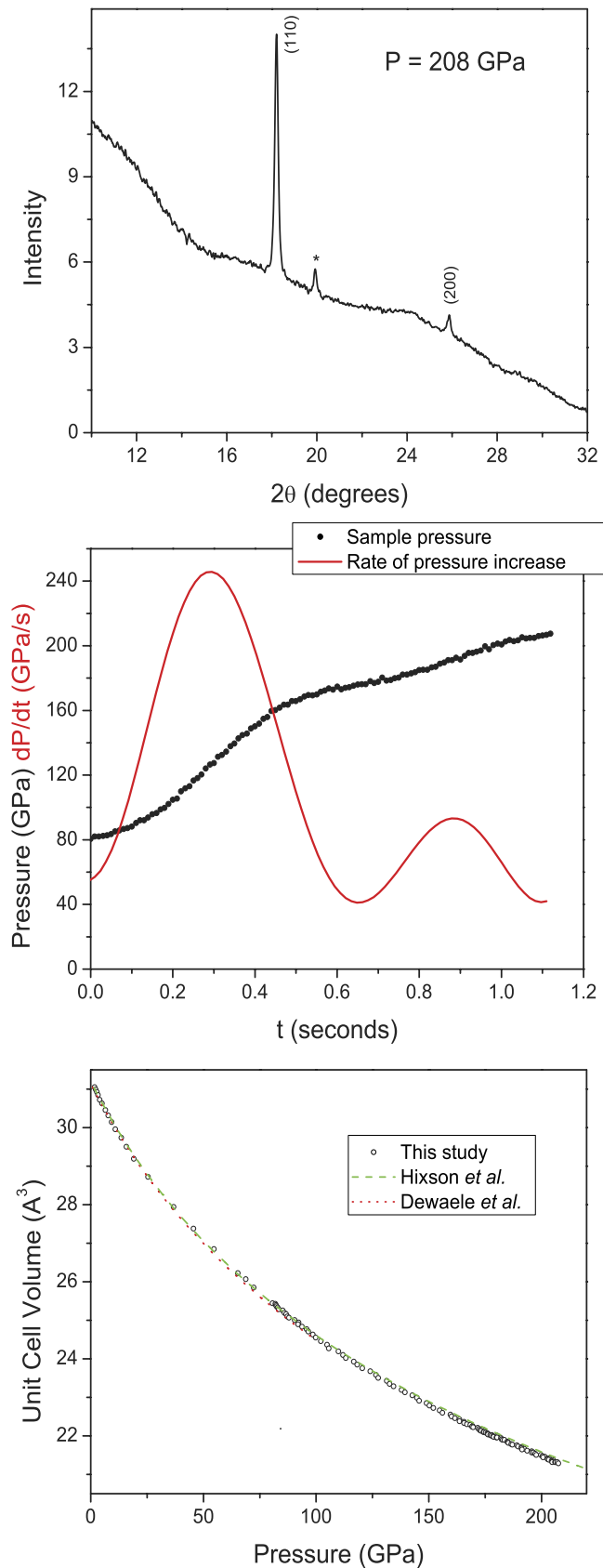


FIG. 2. Ramp compression of molybdenum. (Top) Diffraction pattern obtained at ultrahigh pressure (208 GPa) with 7 ms exposure time. The Mo peaks are indexed, and the (200) peak of MgO used to calculate pressure is indicated by an asterisk. (Middle) Time dependence of the sample pressure (black) and the rate of pressure increase (red) during the 1.13 s pressure ramp. (Bottom) Equation of state of Mo (symbols) compared with reduced shock data (green dashed lines) and best hydrostatic conditions data (red dots).

best hydrostatic conditions¹⁵ and from shock data.¹⁶ A fit to a 3rd order Birch-Murnaghan equation of state yielded $B_0 = 271(2)$ GPa, $B_0' = 3.68(2)$, and $V_0 = 31.18(2)$ \AA^3 . The fitted bulk modulus and its pressure derivative are in agreement with Ref. 15 within the uncertainty of the fit.

Considering the gasket-free image at ultrahigh pressure, it is clear that with careful preparation, ramp compression can be carried out without significant lateral sample displacement. An ultimate pressure of 200 GPa is consistent with what would be expected considering the culet and gasket dimensions. It is unclear what gives rise to the wide and varying rate of pressure increase. It could be due to a number of factors including conductance of the pneumatic system, changes in the sample chamber dimensions (e.g., work on the gasket resulting in time-dependent differences in lateral and compressive flow), or changes in how the DAC and/or diamond anvils deform at ultrahigh pressure. Considering these various factors, it may be quite difficult in practice to achieve a constant ramp (or similarly, strain) rate over a large pressure range and/or time scale. For an average strain rate, the decrease in Mo lattice parameter of almost 6% over a period of 1.13 s yields a strain rate of $5 \times 10^{-2} \text{ s}^{-1}$. For the maximum instantaneous strain rate of Mo at around 118 GPa, a decrease in lattice parameter of about 0.1% over 10 ms corresponds to a strain rate of $1 \times 10^{-1} \text{ s}^{-1}$.

This particular experiment did not strictly require “fast” compression or a time-resolved approach. In fact, the excellent agreement of the resulting equation of state with the equations of state obtained from reduced shock data and conventional static data suggests that the rapid compression did not influence the pressure-volume measurements. There are, however, qualitative and quantitative benefits from this type of experiment. By collecting a large number of data points, it is possible to have a more precise and robust fit for an equation of state. As the pressure steps get smaller, it is easier to detect subtle changes in the compression curve which could be an indication, for example, of a subtle structural change or a detrimental change in the experimental configuration. Also, collecting data over a relatively short period of time could be very beneficial, for example, in thermal equation of state measurements for which it is difficult to maintain extreme (low or high) temperatures for an extended period.

B. Ramp decompression (pneumatic)

Germanium and silicon both adopt a diamond cubic (dc) structure at ambient conditions and upon increasing pressure, both transform to the metallic β -Sn structure at around 12 GPa.¹⁷ Interestingly, this transition pathway is not reversible. Upon slow decompression, Si transforms first to a rhombohedral (R8) phase and then subsequently to a body-centered cubic (bc8) phase which can be retained at ambient conditions.¹⁸ The structural sequence of Ge upon decompression from the β -Sn phase has only recently been clarified. At ambient temperature, there are reports of recovering a simple tetragonal phase upon slow decompression¹⁹ and the bc8 phase (as seen in Si) following rapid decompression.²⁰ Some reports, for example, Lyapin *et al.*,²¹ suggest the formation of the intermediate R8 phase preceding the bc8 phase, but

the pathway, stability, and purity remain unclear. Johnson *et al.* recently demonstrated the formation of R8 germanium based on Raman spectroscopy of samples recovered following unloading in a diamond indentation apparatus.²² To investigate the possible role of the unloading rate in the formation of R8 Ge, and to corroborate their Raman data with diffraction data, members of the same research group carried out time-resolved high pressure powder x-ray diffraction measurements on Ge at HPCAT using various decompression rates.

Commercially prepared crystalline Ge powder was loaded into symmetric DACs together with gold as a pressure marker and neon as a pressure transmitting medium. For each sample, pressure was increased until the sample transformed completely to the metallic phase (in the range of 15-20 GPa) after which a decompression membrane assembly was used to unload the samples down to room pressure over various periods ranging from less than 1 s to almost 1 h. A more detailed account of the sample preparation, experimental procedure, and results has since been published by Haberl *et al.*²³ We here summarize some of the key results and broader implications.

Figure 3 (reproduced from Ref. 23) shows the unexpected result that the R8 phase of Ge was observed in each instance of ramp decompression, regardless of the unloading rate. Although this was a negative result in terms of a compression rate dependent pathway, it was nevertheless significant as it ruled out time dependence as an important factor in the synthetic pathway (at least, over this broad range of time scales). This would not have been possible without the ability to carry out these measurements using time-resolved techniques. A sample was prepared from the same starting material *without* any pressure transmitting medium, unloaded from the metallic phase down to ambient pressure over a period of approximately 80 s, and instead of the β -Sn \rightarrow R8 \rightarrow bc8 \rightarrow HD structural evolution, β -Sn transformed directly to St12 Ge which remained stable at room pressure. This leads to the conclusion that the difference in synthetic pathway is due primarily to highly localized strain/sheer which can be magnified or mitigated in the DAC by the absence or presence of a hydrostatic pressure transmitting medium. Another interesting corollary is that hydrostatic conditions can prevail in diamond indenting experiments depending on the shape of the tip, sample material, etc.

C. Step compression (dDAC)

The distinction between ramp compression and step compression is made at the point when, owing to a high compression rate, it is no longer possible to collect meaningful data during the compression stroke. Clearly, this distinction depends on the particular experiment and is determined by one or more related factors including x-ray flux, engineering limits of the pressure control assembly, and/or quantum efficiency and maximum imaging frequency of the detector. In an effort to explore the maximum possible strain rate we could generate and measure using a DAC, we carried out a step compression experiment using the HPCAT dDAC in compression configuration together with a prototype imaging detector operated at 800 Hz.

A mix of Mo and MgO powders similar to that used in Section III A was loaded into a symmetric DAC with beveled

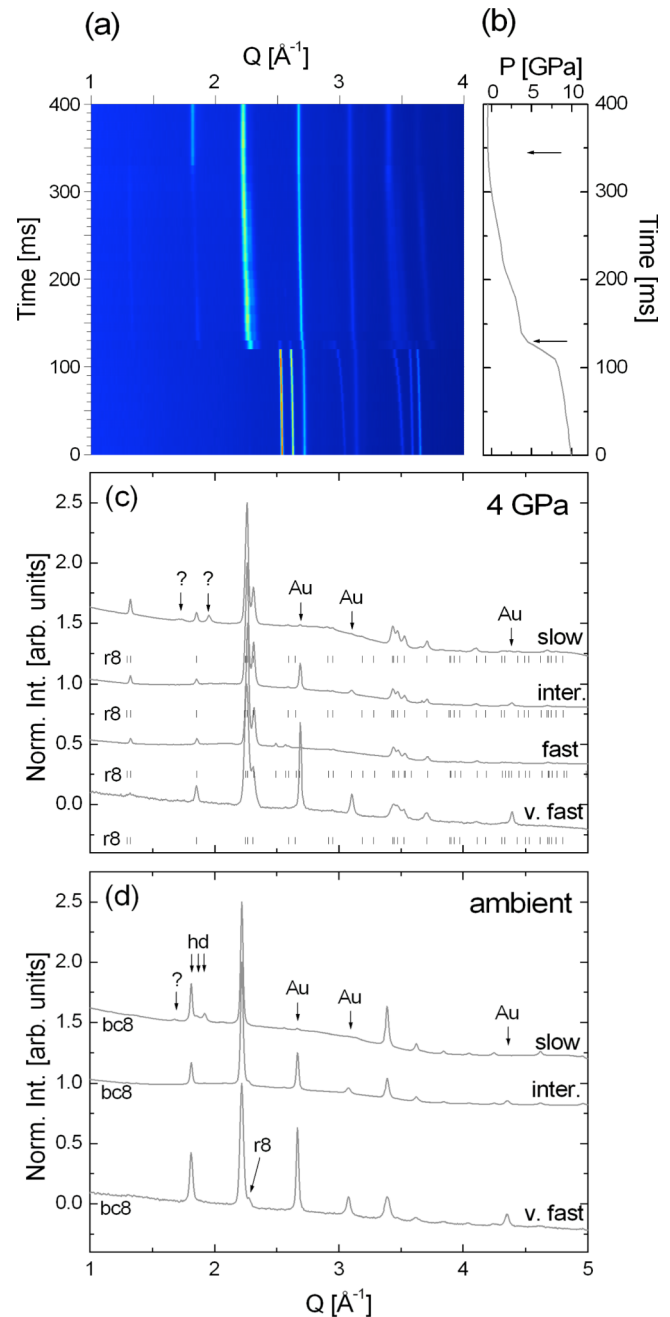


FIG. 3. Synthesis of r8 germanium. (a) Intensity contour plot of all 1D spectra taken during very fast unloading. The phase evolution with time is shown as a function of Q . (b) Pressure dependence of contour plot with respect to time. Spectra at ~ 4 GPa and ambient conditions are indicated with arrows. (c) and (d) X-ray diffraction patterns for the different unloading rates at ~ 4 GPa and upon reaching ambient conditions. Additional phases and elements are marked with arrows, and the r8 peak positions from refinement are indicated by tick marks. The intensities of all spectra were normalized using the dominant r8 and bc8 peaks at 4 GPa and ambient pressure, respectively. For increasing times, the spectra are offset by 0.5 for clarity. Reprinted with permission from Haberl *et al.*, Phys. Rev. B **89**, 144111 (2014). Copyright 2014 American Physical Society.

anvils (250 μm culets, 50 μm flats) and a Re gasket. X-ray diffraction images were collected using a prototype version of DECTRIS' EIGER 1M detector located approximately 95 mm from the sample. Sample pressure was increased manually (pressure screws) up to approximately 100 GPa. The sample was then clamped in the dDAC assembly. The

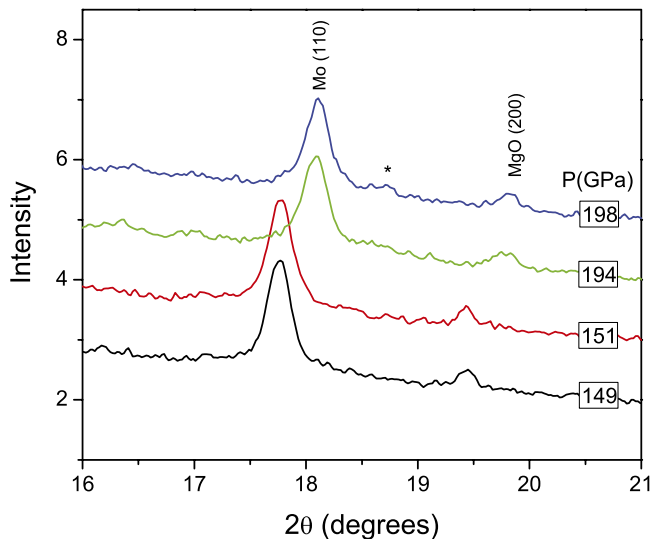


FIG. 4. High strain rate in molybdenum. Four sequential x-ray diffraction patterns taken from a step compression experiment with an imaging frequency of 800 Hz (1.25 ms exposures), demonstrating a strain rate on the order of 10^1 s^{-1} . The asterisk indicates slight contribution from Re gasket.

clamping process involves turning a large threaded collar to initially bring the entire assembly firmly together. To minimize mechanical play in the assembly and to apply some preload to the piezoelectric actuator, the collar is further tightened until the sample pressure increases. To carry out the step compression, we would start the detector imaging sequence (1.25 ms acquire period including approximately $20 \mu\text{s}$ for readout) after which the full 1000 V was at once applied to the piezoelectric actuator to get maximum extension (and hence, maximum compression of the DAC) in the minimum period of time.

Figure 4 shows portions from four sequential diffraction patterns from a single step compression experiment. The observed count rate is similar to that observed for the ramp compression experiment (one count/pixel/ms for the most intense peak of molybdenum). A pressure step of 43 GPa over 1.25 ms corresponds to a compression rate of over 34 TPa/s. Similarly, a decrease in the lattice parameter of Mo by almost 2% over the same time period yields a strain rate on the order of 10^1 s^{-1} .

We here suggest that this measurement is sample and/or detector limited. There is likely an ideal set of initial sample parameters—sample material, gasket material and thickness, initial pressure, etc.—that would yield an even higher strain rate using an otherwise identical experimental procedure. Similarly, the signal-to-background ratio is still sufficiently large to facilitate using an even higher imaging frequency. With these factors in mind, it is reasonable to suggest that a measured strain rate of 10^2 s^{-1} could be readily observed in the DAC at a high energy, 3rd generation synchrotron source.

D. Step decompression (pneumatic)

Returning to the Group IV elements, in the case of Si, it is clear when decompressing from the high pressure phases, the

series of phase transformations and possible phases recovered at ambient conditions may depend on a number of factors including starting material, unloading rate, and/or the degree of hydrostaticity of the sample (see, for example, the introduction to Ref. 24 and references therein). We revisited this line of inquiry to explore what phases could be obtained upon rapid unloading of Si in a DAC and found that under hydrostatic pressure conditions, rapid unloading of the simple hexagonal (sh) phase of Si (Si-V) could result in either crystalline or amorphous phases recovered at ambient conditions, depending on the unloading rate.

For each decompression measurement, a piece of single-crystal Si wafer and a ruby sphere were placed into a symmetric DAC. Samples were gas loaded²⁵ with neon as a pressure transmitting medium, after which pressure was manually increased to over 20 GPa to ensure complete transformation to the (sh) structure. A dDAC would be ideal to achieve the highest decompression rates, but because of the limited stroke, it is not always possible to decompress the sample from 20 GPa down to ambient pressure. Instead, we used a pneumatic diaphragm assembly configured for decompression. To facilitate the highest decompression rate, we used a small solenoid-activated rapid (de)compression apparatus that dumps pressurized gas from a small, secondary lecture bottle into the diaphragm. (This apparatus was also described by Velisavljevic and coworkers²⁶ and is described in more detail elsewhere in this volume.¹¹) Sample pressure was measured using ruby fluorescence²⁷ with an in-house optical system and software

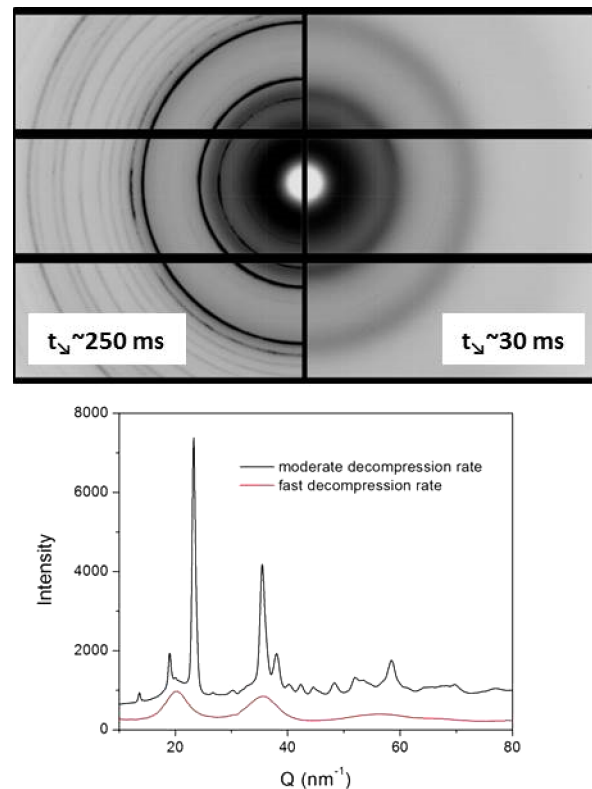


FIG. 5. Synthesis of amorphous Si. (Top) X-ray diffraction images after rapid unloading of Si from a pressure of approximately 20 GPa. A decompression time of $\sim 250 \text{ ms}$ yields crystalline Si (top left), whereas a decompression time of $\sim 30 \text{ ms}$ yields amorphous Si (top right). (Bottom) X-ray diffraction patterns corresponding to the images shown at top.

capable of measuring ruby fluorescence at a rate of 200 Hz. Following rapid decompression down to ambient conditions, samples were characterized using x-ray diffraction. Note that because of the relatively weak scattering of Si, the relatively fast decompression rates, and the choice to use ruby for pressure measurement, it was not feasible to carry out diffraction during decompression.

Figure 5 shows some selected results from the step decompression runs. The top of Fig. 5 compares images collected following decompression times of ~ 250 ms (left) and ~ 30 ms (right). In the case of the left half of the image, the relatively slower decompression from ~ 20 GPa down to ambient pressure conditions yielded crystalline Si (bc8). In the case of the right side of the image, the relatively faster decompression yielded pure, amorphous Si. Fig. 5, bottom, shows the resulting diffraction patterns from the two samples. Although there appears to be a slight amorphous component for the more moderate decompression rate, the sample is primarily crystalline. The data for the pure amorphous sample show no crystalline contribution.

IV. DISCUSSION AND CONCLUSION

From the examples above, it is clear that there are a number of research avenues that are now possible using high pressure x-ray diffraction with rapid DAC (de)compression at HPCAT. However, the examples also give rise to a number of challenges associated with future developments. Considering the measured intensity for the examples with high-frequency imaging, generating and measuring the highest possible strain rates in a DAC while at the same time maintaining or improving the signal-to-background ratio will require significantly more counts on the detector. This challenge is currently being met both in terms of enhanced beam delivery and detector development. Given the ongoing development of next generation, diffraction limited storage rings,²⁸ and complementary advances in APS undulator design,²⁹ it is reasonable to expect at least an order of magnitude increase in flux on the sample over the next several years. The requisite advances in detector technology have already been made; at the time of writing, there are commercial products available with improved imaging frequency and/or quantum efficiency compared to those used in this work. In the coming years, we will see progressively higher diffraction intensities measured during progressively shorter exposure times.

Herein, we have demonstrated a maximum measured strain rate on the order of 10^1 s⁻¹. With the expected significant flux improvements of at least an order of magnitude and similarly with the currently available increase in detector frequency of an order of magnitude, it is reasonable to expect measured strain rates in a DAC on the order of 10^2 - 10^3 s⁻¹. A maximum strain rate of this order would constitute a crucial benchmark as it would overlap with the minimum strain rates that can be achieved using apparatus commonly employed by the dynamic (shock) compression community, for example, Kolsky bar or gas gun. It would also provide experimental access to the intermediate strain rate gap of 10^0 - 10^2 s⁻¹ which cannot be easily and routinely achieved using existing apparatus.³⁰ The DAC could potentially provide a continuous range

of strain rates from arbitrarily low (viz., the static case) up to and including the minimum strain rates generated by the dynamic high pressure community.

One challenge that cannot be easily met is that of precise and predetermined control of the (de)compression/strain rate. The gas pressure for the diaphragm and the voltage for the dDAC can be well-controlled as a function of time. However, the situation remains somewhat complex as the response of the DAC, and thus, sample pressure depends on several factors including the overall DAC design as well as the dimensions and pressure-dependent response of the sample/gasket/anvils system. The general or expected performance of a *particular* DAC may be anticipated after repeated use under similar conditions. With this in mind, it may be beneficial to work toward standardizing some experimental configurations. Dedicated DACs (or similarly, DAC designs), diamond anvil culet dimensions, gasket materials and dimensions, and so forth can be established for some basic pressure ranges and pressure ramp profiles.

As mentioned above, limited software suitable for batch processing of large volumes of high pressure x-ray diffraction data will remain a challenge for the near future. For the examples presented in this work, we have been careful in selecting high symmetry materials for both sample and pressure marker, ensuring there is no peak overlap over a wide pressure range. Automated peak fitting is conceptually straightforward for these cases. The next reasonable step should likely accommodate overlapping peaks, possibly through a whole-pattern fitting approach, opening up this type of investigation to lower-symmetry materials and multiphase samples.

In summary, we have described the key components which enable time-resolved high pressure x-ray diffraction using rapid (de)compression of a DAC at HPCAT and have demonstrated some of the many possible types of measurement that can be carried out using this large-scale apparatus. With current capabilities and future developments, a wide range of strain rates, from the static case up to 10^2 s⁻¹ or more, can be investigated using a DAC at a synchrotron radiation facility. This overlaps nicely with the higher strain rates which will remain the purview of 4th generation light sources and the dynamic high pressure community.

ACKNOWLEDGMENTS

We are grateful to Dr. Przemyslaw Dera for modifying his GSE_shell code specifically to enable data analysis presented in this work. The authors wish to thank DECTRIS for providing the EIGER 1M prototype, and we appreciate the assistance of Matthew Moore, Russell Woods, and Timothy Madden of the APS Detector Pool in facilitating its installation at the beamline. The authors appreciate the assistance of Sergey Tchakev in gas loading some samples. Use of the COMPRES-GSECARS gas loading system was supported by COMPRES under NSF Cooperative Agreement No. EAR 11-57758 and by GSECARS through NSF Grant No. EAR-1128799 and DOE Grant No. DE-FG02-94ER14466. This work was performed at HPCAT (Sector 16), Advanced Photon Source (APS), Argonne National Laboratory. HPCAT operations are supported by DOE-NNSA under Award No. DE-NA0001974

and DOE-BES under Award No. DE-FG02-99ER45775, with partial instrumentation funding by NSF. The Advanced Photon Source is a U.S. Department of Energy (DOE) Office of Science User Facility operated for the DOE Office of Science by Argonne National Laboratory under Contract No. DE-AC02-06CH11357.

- ¹Y. X. Zhao, F. Buehler, J. R. Sites, and I. L. Spain, *Solid State Commun.* **59**, 679 (1986).
- ²P. Dera, J. D. Lazarz, V. B. Prakapenka, M. Barkley, and R. T. Downs, *Phys. Chem. Miner.* **38**, 517 (2011).
- ³W. J. Evans, C. S. Yoo, G. W. Lee, H. Cynn, M. J. Lipp, and K. Visbeck, *Rev. Sci. Instrum.* **78**, 073904 (2007).
- ⁴J. Y. Chen and C. S. Yoo, *Proc. Natl. Acad. Sci. U. S. A.* **108**, 7685 (2011).
- ⁵G. W. Lee, W. J. Evans, and C. S. Yoo, *Phys. Rev. B* **74**, 134112 (2006).
- ⁶G. W. Lee, W. J. Evans, and C. S. Yoo, *Proc. Natl. Acad. Sci. U. S. A.* **104**, 9178 (2007).
- ⁷D. Tomasino and C. S. Yoo, *Appl. Phys. Lett.* **103**, 061905 (2013).
- ⁸P. Kirkpatrick and A. V. Baez, *J. Opt. Soc. Am.* **38**, 766 (1948).
- ⁹W. B. Daniels and M. G. Ryschkewitsch, *Rev. Sci. Instrum.* **54**, 115 (1983).
- ¹⁰R. Letoullec, J. P. Pinceaux, and P. Loubeyre, *High Pressure Res.* **1**, 77 (1988).
- ¹¹S. V. Sinogeikin, J. S. Smith, E. Rod, C. Lin, C. Kenney-Benson, and G. Shen, *Rev. Sci. Instrum.* **86**, 072209 (2015).
- ¹²The object on loan was a prototype of the EIGER 1M detector system with limited functionality and performance compared to the serial model.
- ¹³A. P. Hammersley, S. O. Svensson, M. Hanfland, A. N. Fitch, and D. Hausermann, *High Pressure Res.* **14**, 235 (1996).
- ¹⁴S. Speziale, C. S. Zha, T. S. Duffy, R. J. Hemley, and H. K. Mao, *J. Geophys. Res.: Solid Earth* **106**, 515, doi: 10.1029/2000JB900318 (2001).
- ¹⁵A. Dewaele, M. Torrent, P. Loubeyre, and M. Mezouar, *Phys. Rev. B* **78**, 104102 (2008).
- ¹⁶R. S. Hixson and J. N. Fritz, *J. Appl. Phys.* **71**, 1721 (1992).
- ¹⁷J. C. Jamieson, *Science* **139**, 762 (1963).
- ¹⁸J. Crain, G. J. Ackland, J. R. Maclean, R. O. Piltz, P. D. Hatton, and G. S. Pawley, *Phys. Rev. B* **50**, 13043 (1994).
- ¹⁹F. P. Bundy and J. S. Kasper, *Science* **139**, 340 (1963).
- ²⁰R. J. Nelmes, M. I. McMahon, N. G. Wright, D. R. Allan, and J. S. Loveday, *Phys. Rev. B* **48**, 9883 (1993).
- ²¹A. G. Lyapin, V. V. Brazhkin, S. V. Popova, and A. V. Sapelkin, *Phys. Status Solidi B* **198**, 481 (1996).
- ²²B. C. Johnson, B. Haberl, S. Deshmukh, B. D. Malone, M. L. Cohen, J. C. McCallum, J. S. Williams, and J. E. Bradby, *Phys. Rev. Lett.* **110**, 085502 (2013).
- ²³B. Haberl, M. Guthrie, B. D. Malone, J. S. Smith, S. V. Sinogeikin, M. L. Cohen, J. S. Williams, G. Y. Shen, and J. E. Bradby, *Phys. Rev. B* **89**, 144111 (2014).
- ²⁴B. Haberl, M. Guthrie, S. V. Sinogeikin, G. Shen, J. S. Williams, and J. E. Bradby, *High Pressure Res.* **35**, 99 (2015).
- ²⁵M. Rivers, V. B. Prakapenka, A. Kubo, C. Pullins, C. M. Holl, and S. D. Jacobsen, *High Pressure Res.* **28**, 273 (2008).
- ²⁶N. Velisavljevic *et al.*, "18th Aps-Sccm and 24th Airapt," *J. Phys.: Conf. Ser.* **500**, 1–19 (2014).
- ²⁷H. K. Mao, J. Xu, and P. M. Bell, *J. Geophys. Res.: Solid Earth* **91**, 4673, doi: 10.1029/JB091iB05p04673 (1986).
- ²⁸M. Bei *et al.*, *Nucl. Instrum. Methods Phys. Res. Sect. A* **622**, 518 (2010).
- ²⁹Y. Ivanyushenkov, C. Doose, J. Fuerst, Q. Hasse, M. Kasa, and Y. Shiroyanagi, *IEEE Trans. Appl. Supercond.* **24**, 4102004 (2014).
- ³⁰K. T. Ramesh, *Handbook of Experimental Solids* (Springer, 2012).